Materials Characterization 136 (2018) 398–406

Contents lists available at ScienceDirect

Materials Characterization

journal homepage: www.elsevier.com/locate/matchar

Investigations of γ′, γ″ and δ precipitates in heat-treated Inconel 718 alloy fabricated by selective laser melting

G.H. Cao[a,*], T.Y. Sun[a], C.H. Wang[a], Xing Li[a], M. Liu[a], Z.X. Zhang[a], P.F. Hu[a], A.M. Russell[b], R. Schneider[c], D. Gerthsen[c], Z.J. Zhou[d], C.P. Li[d], G.F. Chen[d,*]

[a] State Key Laboratory of Advanced Special Steel & School of Materials Science and Engineering, Shanghai University, 149 Yanchang Road, Shanghai 200072, China
[b] Department of Materials Science and Engineering, Iowa State University and Division of Materials Science and Engineering, Ames Laboratory of the U.S.D.O.E., Ames, IA 50011-2300, USA
[c] Laboratorium für Elektronenmikroskopie, Karlsruher Institut für Technologie, D-76128 Karlsruhe, Germany
[d] Materials & Manufacturing Qualification Group, Corporate Technology, Siemens Ltd., China, Beijing 100102, China

ARTICLE INFO

Keywords:
Nickel alloys
Selective laser melting
Inconel 718
Microstructure
Transmission electron microscopy (TEM)

ABSTRACT

Inconel 718 alloy samples were fabricated by selective laser melting (SLM). Microstructure and precipitation in solution-heat-treated- and double-aging-SLM-made Inconel 718 were studied by scanning and transmission electron microscopy. Electron microscope observations showed that disc-shaped and cuboidal γ″, and circular γ′ precipitates with an average size of 10–50 nm developed within cellular γ austenite matrix. The simulated, experimentally observed electron diffraction patterns, and dark-field imaging further revealed that the precipitation of three variants of γ″ in the γ matrix occurred. The coarser acicular γ″, and globular as well as plate-like δ phases precipitated at grain boundaries and also within the interior of austenite matrix. The morphology, distribution and crystallography of these precipitates and their formation mechanisms were analyzed and discussed.

1. Introduction

Most heat-resistant nickel-based superalloys are hardened by precipitation of γ′ phase, an intermetallic phase based on $Ni_3(Al,Ti)$ with an ordered face-centered cubic (fcc) $L1_2$ structure. The γ′ phase is coherent with the γ-Ni solid-solution matrix. The principal strengthening mechanism is the antiphase boundary hardening arising from the coherent and ordered γ′ phase [1,2]. A few nickel-based alloys such as Inconel 718 and 625 are hardened by precipitation of coherent, ordered metastable γ″ phase, which has a body-centered tetragonal (bct) DO_{22} structure and is based on the composition Ni_3Nb [1–4]. The γ″ phase has a c/a ratio of ~2.04 and grows coherently with the γ matrix in ellipsoidal/disc-shaped morphologies lying on {001} planes, and c-axis is perpendicular to the disc plane corresponding to ⟨001⟩ directions. Thus, three variants of γ″ can be formed [2–4]. The metastable γ″-Ni_3Nb phase is susceptible to transformation during processing or service to the equilibrium δ-Ni_3Nb (orthorhombic DO_a structure) [5].

Inconel 718 alloy has found many industrial applications because of its excellent corrosion-resistant, thermal and strength properties under extreme thermal and mechanical conditions [6,7]. However, Inconel 718 is difficult to machine due to excessive tool wear and low material removal rate, and the segregation of alloying elements in the heat-affected zone around welds degrades strength. Moreover, many Inconel 718 components have complex shapes with mazy inner channels or overhangs making them difficult to manufacture by conventional techniques [7,8]. Selective laser melting (SLM) is a rapid prototype, 3D printing or additive manufacturing (AM) technique used to directly produce metallic parts from powder [9,10]. SLM process enables fabrication of components with complex geometries and overcomes geometric restrictions that exist for conventional manufacturing processes such as casting and forging [11].

During SLM fabrication each layer undergoes rapid solidification when the metal powders are melted by the laser, and the successive layers experience a variety of heating and cooling cycles. The microstructural features after AM processing are different from those of forging and casting [12,13]. Prior studies have shown that a laminar material structure and columnar microstructure are observed in as-fabricated SLM Inconel 718 samples [6–8,11,14]. The predominant texture component is a relatively strong ⟨100⟩ fibre in the build direction [6,7]. The short interaction times of high energy laser with small spot size and high velocity in localized areas result in large thermal gradient and, consequently, in high thermal stresses during

* Corresponding authors.
E-mail addresses: ghcao@shu.edu.cn (G.H. Cao), guofeng.chen@siemens.com (G.F. Chen).

https://doi.org/10.1016/j.matchar.2018.01.006
Received 6 October 2017; Received in revised form 2 January 2018; Accepted 3 January 2018
Available online 05 January 2018
1044-5803/

SLM process. The existence of thermal stress makes materials unstable [14,15]. Rapid solidification of thin layers by high cooling rate leads to the directional grain growth, microsegregation of high concentration refractory elements such as Nb and Mo and formation of non-equilibrium phases, including carbides and Laves phases, known for degrading mechanical properties [14,16]. The precipitation of the strengthening γ′ and γ″ phases is inhibited [17]. Therefore, post heat treatments are needed to optimize the microstructure of the SLM-made materials to meet the requirements of working conditions. The heat treatments of Inconel 718 alloy consist of homogenization or solution plus double aging treatments. The homogenization or solution annealing can promote the diffusion of segregation elements and dissolve the brittle phases such as carbides and Laves phases into the austenite matrix, and aging treatments are intend to form the strengthening γ′ and γ″ precipitates. There are plenty of researches on heat-treated Inconel 718 alloy fabricated by SLM, but most of them are concentrated on heat treatment processes, carbides, Laves and δ-Ni_3Nb phases [14–17], and only few pay attention to the study of the strengthening γ′ and γ″ phases [6] and their crystallographic relations with austenite matrix probably due to their nano-scale precipitations resulting in the difficulties to identify the individual structure. For the heat-treated specimen, the plate-like δ-Ni_3Nb precipitates appear at grain boundaries and inside the grains [6,8,11,14–17], and the γ′ and γ″ phases are too small to be clearly resolved even by high-resolution scanning electron microscopy (SEM) [8,18]. The TEM work by Amato et al. [6] has shown γ″ precipitates – < 35 nm in SLM-processed Inconel 718 specimens annealed in argon at 1160 °C for 4 h. However, rather limited information has been published on the precipitate morphologies, their crystallographic structures and the orientation relationships of the γ′, γ″ and δ phases with the γ matrix in the heat-treated Inconel 718 alloy prepared by SLM.

The work reported in this paper is to investigate the microstructure of heat-treated Inconel 718 processed by SLM via X-ray diffraction (XRD), SEM and TEM. Emphasis is placed on studying the precipitation of intermetallic γ′, γ″ and δ phases in Inconel 718. Such a study is expected to be helpful in understanding the microstructural development and mechanical behavior of Inconel 718 fabricated by SLM.

2. Experimental Procedure

Commercial Inconel 718 powders were used as the starting materials in SLM experiments. Fig. 1 is a SEM image showing the powder morphology, with an average particle size of 20 to 50 μm. The manufacturing of the samples was performed in an EOSINT M280 machine operated at a power of ~285 W with a scanning speed of 0.96 m/s, laser focus spot size of 70 μm, and laser thickness of 40 μm [19]. The as-built cylindrical samples were 10 mm in diameter and 100 mm long in total, which were solution heat-treated at 1065 °C for 1 h, followed by air cooling. Then, the double aging was carried out at 760 °C for 10 h followed by furnace cooling for 2 h to 650 °C and holding at 650 °C for 8 h, and finally air cooling to room temperature. The chemical compositions (at.%) of the heat-treated Inconel 718 alloy analyzed by inductively coupled plasma optical emission spectrometry is 54.22Ni-20.21Cr-3.33Nb-2.33Mo-1.09Ti-1.72Al-Fe (balance).

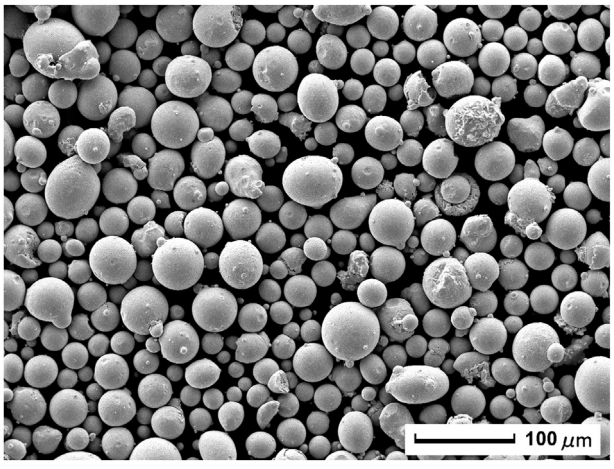

Fig. 1. SEM image showing Inconel 718 powder morphology with an average particle size of 20 to 50 μm.

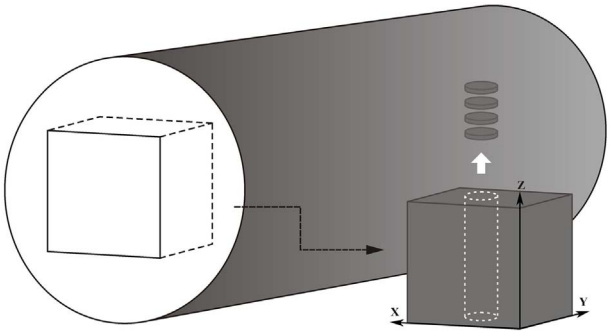

Fig. 2. Sketch showing cylindrical sample and the positions of the cube and pin taken for microstructural analysis, the axis of *z* is the build direction.

Fig. 2 is a sketch of a cylindrical sample, the axis of *z* is the build direction. To investigate the microstructure, a cubic specimen (Fig. 2) with a side length of ~8 mm was prepared by electrical-discharge machining (EDM) and mechanically polished via a standard metallographic procedure using 1 μm diamond powder in the final stage of polishing. After final electropolishing the specimen was etched in a solution composed of 70 vol% H_3PO_4 and 30 vol% H_2O at 5 V at room temperature. The microstructure of the etched specimen was examined by a JSM-7001 SEM. The phase constitutions of the alloy were determined by a D/MAX-3C X-ray diffractometer with Cu K_α radiation in the range $2\theta = 20–100^\circ$ with a step size of 0.02° and a counting time of 1 s per step. A small pin (Fig. 2) with a diameter of 3 mm was prepared by EDM with the pin's cylindrical axis parallel to the longitudinal building direction. Discs 3 mm in diameter (*xy* plane) and ~0.2 mm in thickness (*z* axis) were cut from the pin by EDM. TEM specimens were prepared by grinding discs to a thickness of ~80 μm and electropolishing in a twin-jet apparatus using an etchant consisting of 10 vol% perchloric acid and methanol solution at 25 V and a temperature of − 25 °C. TEM bright-field (BF)/dark-field (DF) imaging and selected area electron diffraction (SAED) were performed in Philips CM 200 ST, JEOL 2010F and JEOL 2100F electron microscopes equipped with field emission guns and operated at an accelerating voltage of 200 kV. Simulation of the electron diffraction patterns was carried out with Desktop Microscopic software.

3. Results

The XRD diffractograms of the horizontal (*xy*) and vertical (*yz* and *xz*) planes from heat-treated specimen are shown in Fig. 3. The profiles have similar XRD patterns with strong ⟨200⟩ textures. Since there is a nearly exact γ(111)/γ′(111) peak match as well as matches for γ(200)/γ′(200)/γ″(200), γ(220)/γ′(220)/γ″(220), and γ(311)/γ′(311)/ γ″(033), it is not possible to determine the γ′ and γ″ precipitates from XRD data. Peaks at $2\theta = 47.5^\circ$ could be indexed as the (211) peak of the δ phase. Fig. 4 shows a three-dimensional (3D) SEM image composite corresponding to a section of Fig. 2 illustrating two different types of precipitates. The thickest precipitates with the morphology of short platelets were identified as δ-phase according to the literature [5,18]. The γ″ phase precipitates lying end-on with acicular morphology. Cuboidal and circular precipitates could be γ″ and γ′ phases [2,4]. Therefore, unambiguous identification of the γ′, γ″ and δ precipitates must rely on TEM observations, especially the SAED patterns.